10^{th} International Conference on Fracture Mechanics of Concrete and Concrete Structures
FraMCoS-X
G. Pijaudier-Cabot, P. Grassl and C. La Borderie (Eds)
https://doi.org/10.21012/FC10.235610

TEST INDEPENDENT IDENTIFICATION OF FRACTURE PARAMETERS OF PLAIN CONCRETE BASED ON A COHESIVE XFEM FORMULATION

YUNUS EMRE HARMANCI*, KONSTANTINOS AGATHOS*, GIL JACOT-DESCOMBES† AND ELENI CHATZI*

Swiss Federal Institute of Technology
Zürich, Switzerland
e-mail: *{harmanci, agathos, chatzi}@ibk.baug.ethz.ch, †gilj@student.ethz.ch

Key words: Cohesive Fracture, XFEM, fracture energy

Abstract. Based on current procedures, identification of fracture parameters, and in particular traction separation laws, for concrete is performed by means of fitting analytical models to experimental results. To this end, specialized experiments need to be designed and appropriate analytical models, representing the specific test setup, have to be employed. However, performing such experiments can be quite involved due to the constraints imposed by testing standards, equipment and the identification procedure itself. Additionally, the inference of adequate analytical models that accurately represent the experimental setup is a non-trivial task.

In the present work we propose a procedure relying on numerical, rather than analytical, models for the identification process aiming at relaxing some of the requirements typically imposed by conventional methods. More specifically, numerical models can be generated for arbitrary geometries and loading conditions, thus providing flexibility with respect to the corresponding experimental set up. Moreover, numerical models can account for a wide variety of traction separation laws with ease, allowing for more flexibility in the identification process. In contrast, analytical models are subject to very specific assumptions.

The numerical method used in the proposed procedure is the extended finite element method (XFEM) for cohesive fracture. Although other alternatives might also prove adequate, the XFEM allows to model cracks of arbitrary geometries independently of the mesh used and in an automated fashion, thus constituting an ideal candidate for incorporation in the proposed scheme. To identify fracture parameters, the XFEM model is coupled with optimization algorithms and validated against physical and numerical experiments.

1 INTRODUCTION

The softening (failure) behaviour of concrete can be utilized to model the cracking behaviour in numerical simulations [1], [2], [3]. This behaviour is assumed quasi-brittle, and can be represented with the cohesive crack model by employing traction-separation ($\sigma-$w) laws, as proposed by Hillerborg et al. [4]. Adequate estimation of this law may allow simulations of enhanced precision and can ensure safe design. The majority of currently employed techniques to estimate the traction-separation laws rely on fitting an analytical or numerical model to test data by modifying the input parameters and comparing resultant global force-displacement responses. Depending on differences in the testing geometry, boundary and loading conditions, analytical models may require test- and material-dependent considerations. The use of numerical analysis tools, such

as the finite element method (FEM), may be considered as a more generalized alternative, yet no well-defined framework has been established for this purpose. The sensitivity to experimental uncertainties and potential existence of local minima within the search space of the optimization problem can also manifest themselves as disruptive effects on the accuracy of such approaches. Some examples of $\sigma-$w estimation schemes within the literature include an analytical formulation based on the cracked hinge model [5], approximating the traction-separation law by a piece-wise linear function [6, 7], J-integrals [8], and FEM [9, 10].

Although uniaxial tensile tests can directly deliver the σ-w relationship, extensive experimental considerations are required, which is non-practical in case of absence of specialized testing equipment [11]. Various other tests, necessitating less specialized testing equipment, can be utilized to obtain an indirect estimate of mode-I cohesive fracture parameters. The most commonly used methods are reported to be the three point bending test (TPBT) [12] and the wedge split test (WST) [13]. The load application can be controlled either via stroke-displacements or, as a more stable alternative, crack mouth opening displacements (CMOD). Measured force and crack mouth opening displacements can then be employed to identify the necessary parameters.

This study proposes a generalized configuration-independent framework to obtain fracture parameters of plain concrete via the use of the eXtended Finite Element Method (XFEM)[14, 15] coupled with the co-variance matrix adaptation evolution strategy (CMA-ES) [16, 17]. The proposed scheme is validated with three point bending test (TPBT) results of single edge notched beam (SENB) specimens. Since the only inputs required by the framework pertain to specimen geometry, loading and boundary conditions, a wide variety of tests can be utilized for fracture parameter estimation without the need to rely on very specific testing protocols/equipment, as well as on case-specific analytical formulations.

2 EXPERIMENTAL INVESTIGATIONS

An experimental campaign was launched to obtain the fracture characteristics of concrete via three-point bending tests on plain concrete single edge notched beams. The specimens further underwent accelerated ageing conditions, namely carbonation and freeze-thaw-cycles, as part of a durability investigation, which falls out of scope and will not be further mentioned herein. Interested readers are referred to the work of Harmanci et al. [18, 19] for further details.

A concrete mixture was designed according to EN 206-1 [20], considering cyclic wet and dry condition (XC4) and freeze-thaw attack due to the constant high water saturation (XF3). To this end, a Portland-limestone cement according to EN 197-1 [21] (CEM II/A-LL 42.5 N), well-rounded alluvial gravel with a maximum aggregate size of 16 mm and a water-cement ratio of 0.48 was used. Air entraining admixtures were not used in order to reduce variation within test results. Concrete prisms with dimensions of 120 x 120 x 360 mm^3 (HxWxL) were cast from a single batch, demolded 24 hours after casting and subsequently stored in a climate chamber at 20^{o}C and 90% RH.

When the full cure of cast prisms was ensured via cubic compressive tests, a notch of 5 mm thickness and 30 mm depth was introduced on the top casting surface by a rotary cutter at 191 days of age. In contrast to the dimensions suggested by RILEM [22], a large ligament area of 75% was kept to minimize scatter within test results. The RILEM specifications serve for ensuring applicability on a variety of testing machines, of varying stiffness and stroke-displacement control. The requirement of large span-to-depth ratio disappears under closed-loop crack mouth opening displacement (CMOD) control [23], as employed for the tests reported in this study. For this purpose, the load spplied by the testing machine (Walter+Bai) was controlled via a clip gauge (HBM) attached to two steel wedges on the notched side of the beam. A crack opening rate of 0.005 mm/s was applied in a three point bending test

setup comprising a 320 mm span length. In addition to the CMOD sensor, full-field displacements were measured via a 2D-DIC system, utilizing a conventional DSLR camera. The vertical displacements of the beam were deduced by means of 2D Digital Image Correlation (2D-DIC), in conformance with RILEM recommendations. The test configuration is presented in Figure 1.

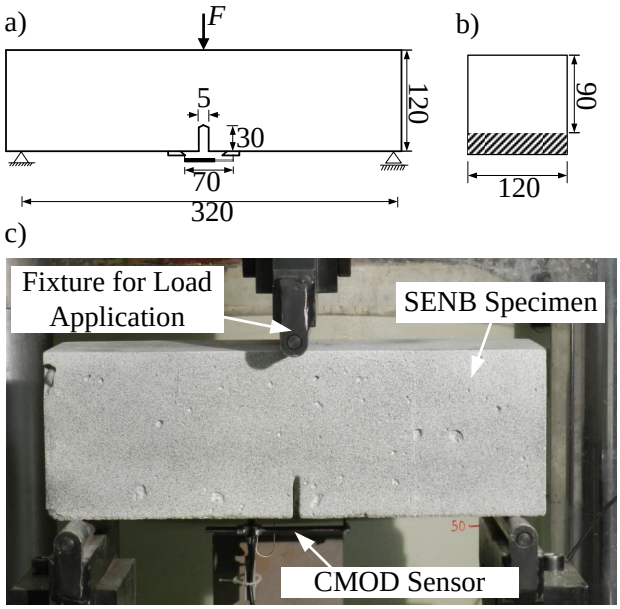

Figure 1: a)Side and b) cross-sectional view of specimens at mid-span and c) test setup. All dimensions are in mm.

3 INVERSE PROBLEM

3.1 Solution of the forward problem using XFEM

The XFEM is employed for the solution of the forward problem due to its ability to represent cracks independently of the underlying finite element (FE) mesh, thus removing the need for remeshing. This feature has already been exploited in the solution of inverse problems, more specifically in crack detection problems in two [24, 25] and three dimensions [26, 27].

3.1.1 Weak form

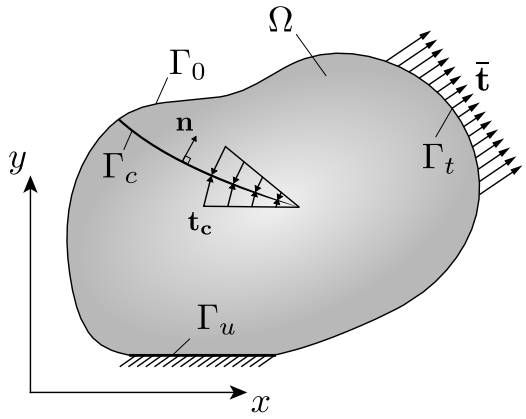

Figure 2: Cracked body, boundary conditions and cohesive forces.

The forward problem consists of a cracked body, as depicted in Figure 3.1.1, occupying a domain Ω, whose boundary Γ is composed of the parts Γ_u, where displacements $\bar{\boldsymbol{u}}$ are prescribed, Γ_t, where surface tractions $\bar{\boldsymbol{t}}$ are applied, and Γ_0 where free surface conditions apply. At part of the crack surface (Γ_c) cohesive forces $\boldsymbol{t}_c$ are applied in the direction normal to the crack surface, defined by vector $\boldsymbol{n}$.
Find $\boldsymbol{u} \in \mathcal{U}$ such that $\forall \boldsymbol{v} \in \mathcal{V}^0$

$$\int_\Omega \boldsymbol{\sigma}(\boldsymbol{u}) : \boldsymbol{\epsilon}(\boldsymbol{v})\, d\Omega + \int_{\Gamma_c} \boldsymbol{t}_c\left(\boldsymbol{w}_{\boldsymbol{u}}\right) \cdot \boldsymbol{w}_{\boldsymbol{v}}\, d\Gamma_c = \tag{1}$$

$$= \lambda \int_{\Gamma_t} \bar{\boldsymbol{t}} \cdot \boldsymbol{v}\, d\Gamma_t$$

where $\boldsymbol{\sigma}$ and $\boldsymbol{\epsilon}$ are the stress and strain tensors, $\boldsymbol{w}_{\boldsymbol{u}} = \boldsymbol{u}^+ - \boldsymbol{u}^-$ is the displacement jump along the crack surface and $\boldsymbol{w}_{\boldsymbol{v}} = \boldsymbol{v}^+ - \boldsymbol{v}^-$. The spaces involved are defined as:

$$\mathcal{U} = \left\{ \boldsymbol{u} | \boldsymbol{u} \in \left(H^1(\Omega)\right)^3, \boldsymbol{u} = \bar{\boldsymbol{u}} \text{ on } \Gamma_u \right\} \tag{2}$$

and

$$\mathcal{V}^0 = \left\{ \boldsymbol{v} | \boldsymbol{v} \in \left(H^1(\Omega)\right)^3, \boldsymbol{v} = 0 \text{ on } \Gamma_u \right\} \tag{3}$$

Functions of $H^1(\Omega)$ are implicitly discontinuous along the crack surface.

The bulk of the body is assumed to be linear elastic, thus the engineering strain definition and Hooke's law are used as kinematic and constitutive relations respectively. Cohesive tractions are assumed to be normal to the crack surface:

$$\boldsymbol{t}_c\left(w\right) = \boldsymbol{n}t\left(w\right) \tag{4}$$

where w is the crack opening displacement in the direction normal to the crack surface. The magnitude of the cohesive tractions is given by a bilinear law as illustrated in Figure 3.1.1.

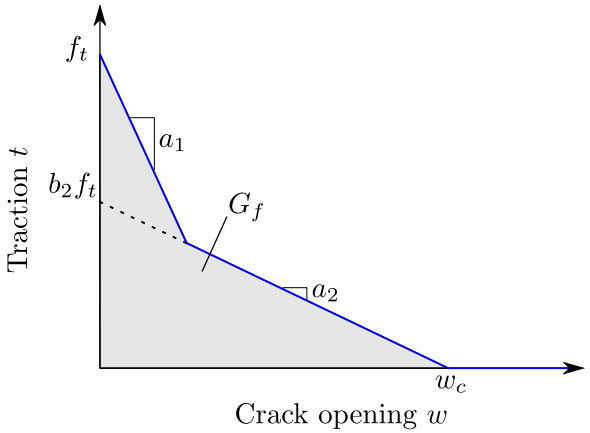

Figure 3: Bilinear traction separation law.

3.1.2 Crack representation

The crack is implicitly represented by level set functions defined as:

- ϕ the signed distance from the crack surface.
- ψ the signed distance from a surface, normal to the crack surface, that intersects the crack surface at the crack tip.

Subsequently, the vector normal to the crack surface can be obtained as the gradient of the first level set function.

For crack propagation, while several update methods are available, in the present work we employ the $\phi\psi r\theta$ method from the work of Duflot [28].

3.1.3 Discretization

The weak form is discretized using the XFEM [14, 15] with shifted enrichment functions [29], leading to the following approximation for the displacements:

$$\begin{aligned}\mathbf{u}\left(\mathbf{x}\right) = &\sum_{I\in\mathcal{N}} N_I\left(\mathbf{x}\right)\mathbf{u}_I \\ &+ \sum_{J\in\mathcal{N}^j} N_J\left(\mathbf{x}\right)\left(H\left(\mathbf{x}\right) - H\left(\mathbf{x}_J\right)\right)\mathbf{b}_J \\ &+ \sum_{T\in\mathcal{N}^t} N_T\left(\mathbf{x}\right)\left(F\left(\mathbf{x}\right) - F\left(\mathbf{x}_T\right)\right)\mathbf{c}_T\end{aligned} \tag{5}$$

where $N_I\left(\mathbf{x}\right)$ are the FE interpolation functions, $\mathbf{x}_I$ are the coordinates of node I, $\mathbf{u}_I$ are FE degrees of freedom (dofs), $\mathbf{b}_J$ and $\mathbf{c}_T$ are enriched degrees of freedom.

The enrichment functions used rely on the modified Heaviside function, allowing to represent displacement jumps along the crack faces:

$$H(\mathbf{x}) = \begin{cases} 1, & \phi \geq 0 \\ -1, & \phi < 0 \end{cases} \tag{6}$$

and a linear branch function, as in the work of Moës and Belytschko [30], allowing to represent the displacement field in the vicinity of the crack tip:

$$F\left(r,\theta\right) = r\sin\frac{\theta}{2} \tag{7}$$

Coordinates r and θ refer to a polar system with its origin at the crack tip and are defined as:

$$r = \sqrt{\phi^2+\psi^2}, \qquad \theta = \arctan\left(\frac{\phi}{\psi}\right) \tag{8}$$

The nodal sets involved in the approximation are defined as:

- $\mathcal{N}$ is the set of all nodes in the FE mesh.
- $\mathcal{N}^j$ is the set of jump enriched nodes. This nodal set includes all nodes whose support is split in two by the crack.
- $\mathcal{N}^t$ is the set of tip enriched nodes. This nodal set includes all nodes whose support includes the crack tip.

3.1.4 Solution of the non-linear equilibrium equations

The weak form of Equation (1) results in a nonlinear system of equations, which is linearized and solved using the Newton-Raphson method as in Zi and Belytschko [29] and Zamani et al. [31]. Since the load factor λ is also treated as an unknown, an additional equation is provided by setting the normal stress to the crack surface at the crack tip equal to the tensile stress of the material [29]:

$$\boldsymbol{n} \cdot \boldsymbol{\sigma} \cdot \boldsymbol{n} = f_{ct} \tag{9}$$

where f_{ct} is the tensile strength of the material.

3.1.5 Crack propagation

For propagating cracks, the procedure described above is repeated for each propagation step. Although in the experiments simulated within the present work the direction of propagation is known due to symmetry, in more complicated cases this can be determined through the stress intensity factors and an appropriate criterion as discussed in Moës and Belytschko [30].

3.2 Solution of the inverse problem using CMA-ES

Using the method described in the previous subsection, the experimental setup can be modelled and load-CMOD curves can be obtained for arbitrary combinations of material parameters. Then, the inverse problem can be posed as an optimization problem, where the material parameters assume the role of design variables and some norm of the difference between the computed and measured load deflection curves assumes the role of the objective function. Herein, the objective function is defined as the mean-squared difference between the experimental and numerical load-CMOD curves. The optimization problem is solved using the (CMA-ES) algorithm [16, 17], an widely used evolutionary algorithm, suitable for non-convex global optimization problems. Parameters f_t, a_1, a_2, b_2 (see Figure 3.1.1) as well as the elastic modulus E are used as design variables. The fracture energy G_f, although not directly identified through the above procedure, can be obtained as the area underneath the traction separation law, as in Figure 3.1.1.

3.3 Reference material parameters

In order to validate the proposed XFEM-based framework, two approaches were chosen as a basis for comparison. An inverse analysis scheme based on the analytical cracked hinge model [32] and the fib Model Code 2010 [33], both established techniques, are employed herein.

3.3.1 Analytical Modelling

The inverse analysis procedure utilizing an analytical model is based on the work of Østergaard et al. [32], coupling the cracked hinge model [34, 35] with the population based stochastic optimization technique Particle Swarm Optimization (PSO) [36], in order to determine parameters that reproduce experimental curves with sufficient accuracy. The cracked hinge model provides an analytical solution for the entire F-CMOD curve, assuming that the material is quasi-brittle and can be described by the fictitious crack model [37]. For any given value of angular deformation of the hinge, the externally applied load as well as CMOD can be calculated. These values are formulated as a function of the aforementioned five parameters, analogously defined for the XFEM-based approach. Similarly, the cost function that is to be minimized to obtain the parameters that reproduce experimental findings is formed as previously mentioned in Section 3.2. Through some modifications within the formulation, the cracked hinge model can also be employed for wedge split tests.

3.3.2 fib Model Code 2010

The *fib* Model Code 2010 [33] is used herein to obtain approximate expected values to assess

the plausibility of identified parameters. Time-dependent elastic modulus is calculated as provided in Equation 10.

$$E_{ci}(t) \quad = \quad \beta_E(t) \cdot E_{ci}, \tag{10}$$

with

$$\beta_E(t) \quad = \quad \left(exp\left\{ s\left[1 - \left(\frac{28}{t} \right)^{1/2} \right] \right\} \right)^{0.5} \tag{11}$$

where the coefficient s is taken as 0.25 based on the strength class of cement, t denotes concrete age in days and the tangent modulus of elasticity E_{ci} at 28 days is given by Equation 12.

$$E_{ci} \quad = \quad \alpha_E \cdot E_{co} \left(\frac{f_{cm}}{10} \right)^{1/3}, \tag{12}$$

where $\alpha_E = 1.0$, $E_{co} = 2.15 \cdot 10^4$ MPa and f_{cm} represents the mean compressive strength.

The mean tensile strength f_{ct} is determined by

$$f_{ctm} \quad = \quad 0.3 \cdot (f_{ck})^{2/3}. \tag{13}$$

Similarly, the fracture energy from compressive tests are determined as

$$G_F \quad = \quad 73 \cdot f_{cm}^{0.18}, \tag{14}$$

which is valid for normal strength concrete.

4 RESULTS AND DISCUSSION

Parameters identified via the numerical and analytical inverse methods as well as the fib guidelines are herein cross-compared. Experimental load-CMOD curves of reference specimens (i.e. no ageing exposure) and specimens that underwent concrete carbonation are also compared against curves obtained through XFEM and the cracked hinge model. The comparison is achieved solely based on observed quantities and as previously mentioned, no discussion is included pertaining to the effects of concrete carbonation on the fracture behaviour.

4.1 3 point bending test

In order to simulate the experiments described in Section 2, the geometry of the specimen of Figure 1 is discretized using an unstructured mesh consisting of 1,382 bi-linear quadrilateral elements and 1,462 nodes, as illustrated in Figure 4.1. The mesh is refined towards the center and the top of the beam. The refinement towards the center is introduced to increase the resolution around the crack, while refinement towards the top aims at more accurately capturing the end of the descending branch of the load deflection curve which corresponds to a crack tip location within that area. Regarding the crack propagation increment, different values are used throughout the simulation to reduce the computational cost and to allow for a more uniform distribution of points along the load deflection curve. More specifically, for the first 10 steps an increment of 3 mm is used, for the subsequent 8 steps an increment of 1 mm is used, and finally for the last 7 steps the increment is set to 0.25 mm. It should be noted that the since in this problem the crack path is straight, subsequent crack propagation steps are not affected by previous ones, thus this selection of increments does not affect the overall behavior of the solution. The deformed configuration depicted in Figure 4.1 (b) corresponds to the tenth crack propagation step.

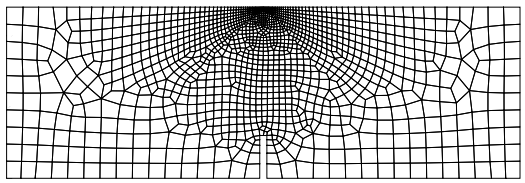

(a)

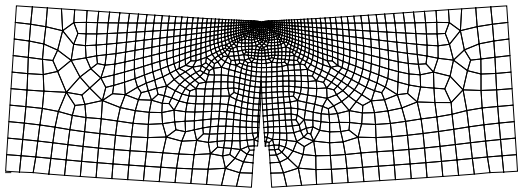

(b)

Figure 4: Mesh used for the three point bending test in (a) undeformed configuration and (b) deformed configuration after 10 crack propagation steps.

For the optimization problem, the default parameters of the CMA-ES algorithm [16, 17] are used, which result in a population size equal to 8. In order to restrict the search space, the lower and upper bounds of Table 4.1 are imposed for the material parameters. Variables are scaled so to assume values in the $[0, 1]$ interval and an initial standard deviation $\sigma = 3$ is used. The algorithm is terminated once the standard deviation for each variable is less than 1% of the initial value.

Table 1: Lower and upper bounds for the identified material parameters.

Parameter	Lower bound	Upper bound
E (MPa)	20,000	65,000
f_{ct} (MPa)	2.000	5.500
a_1 (mm $^{-1}$)	10.000	70.000
a_2 (mm $^{-1}$)	0.100	5.000
b_2	0.001	1.000

In Figure 5, experimental F-CMOD curves of reference beams are plotted against analytical and numerical results. A good match is achieved, reproducing the initial elastic regime, peak loads as well as the descending branch accurately. A similar observation can also be made for the carbonated concrete specimen results presented in Figure 6.

The average values obtained through all three presented methodologies, namely the inverse schemes via XFEM, the cracked hinge model and the values obtained through the fib formulae provided in Equations 10-14 are given in Table 4.1. Moreover, a graphical comparison of the bilinear traction-separation curve obtained both via the analytical and numerical model is presented in Figure 7. It is possible to infer based on these results that the XFEM-based inverse analysis approach complies with both reference techniques. It should be noted that values obtained through the fib Model Code may result in inaccurate predictions if the tested concrete cubes do not fall within the defined specifications dictated by the guideline, hence, potentially limiting its generalized use. Similarly, the cracked hinge model, albeit being a rigorous and accurate methodology, would deem itself as an inflexible approach in case a different test-setup was to be employed. For instance, application to the wedge split test (WST) would be possible via modifications in the formulation, yet a complete test-independent behaviour can only be achieved within a numerical framework.

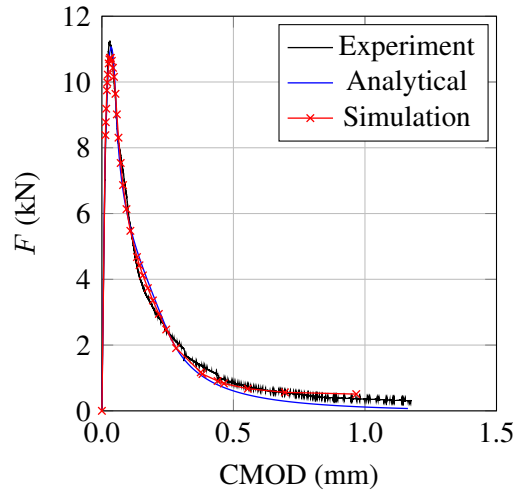

(a)

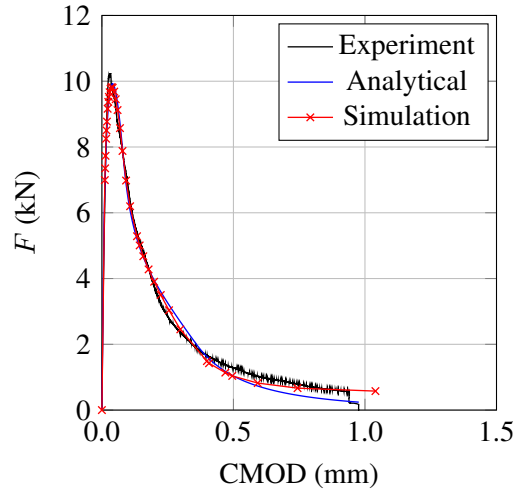

(b)

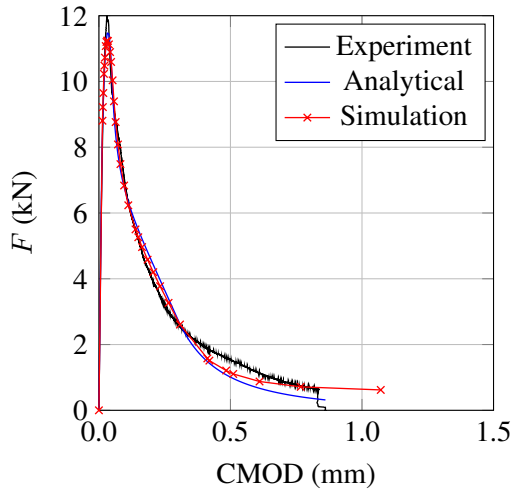

(c)

Figure 5: Load-CMOD curve for the three tested reference specimens.

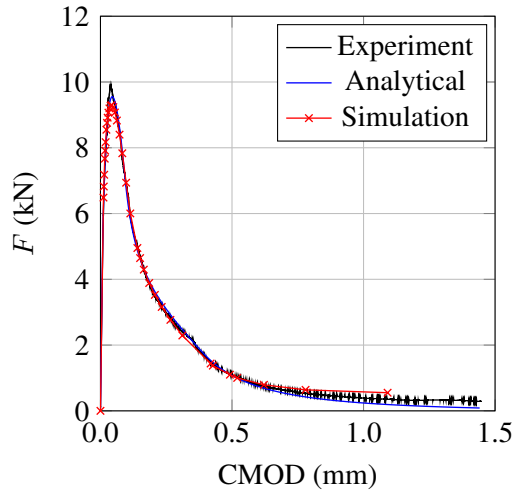

(a)

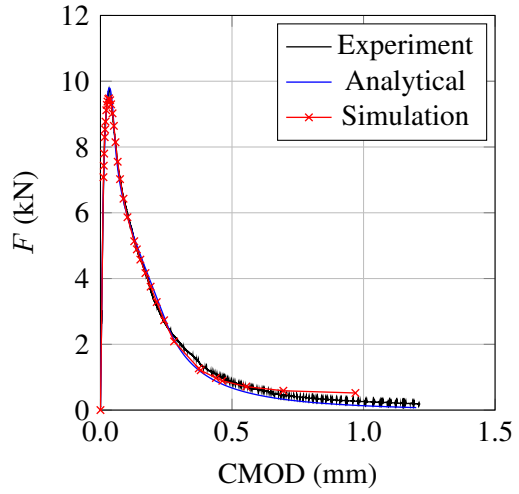

(b)

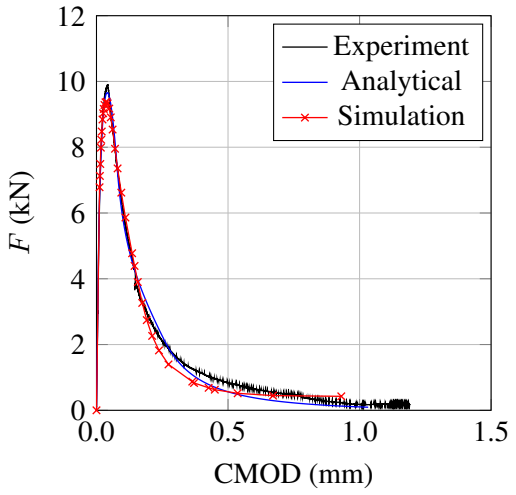

(c)

Figure 6: Load-CMOD curve for the three tested specimens after concrete carbonation.

Table 2: Comparison of identified parameters using the analytical and numerical model.

Parameter	Anal.	Num.	Ref.
E (MPa)	34,978	44,705	39,165
f_{ct} (MPa)	3.222	2.706	4.011
a_1 (mm $^{-1}$)	21.059	16.974	-
a_2 (mm $^{-1}$)	1.549	2.059	-
b_2	0.321	0.309	-
G_f (N/m)	151.185	133.569	148.988

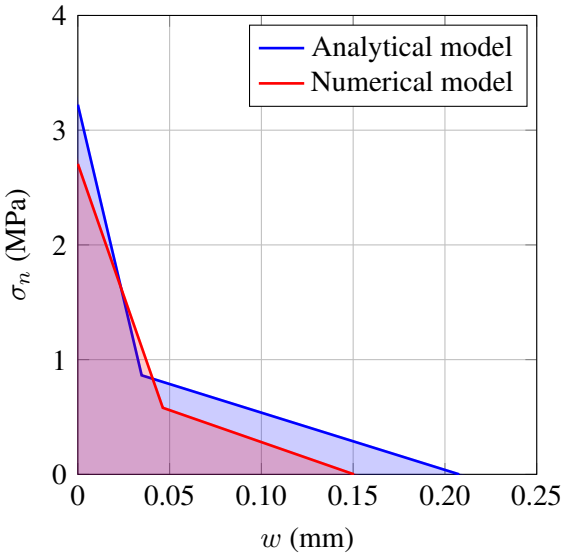

Figure 7: Identified traction separation law using the analytical and numerical model for the reference case.

In Figure 8 the performance of the optimization algorithm is illustrated in terms of evaluations of the forward problem against the value of the RMS difference between the experimental and numerical load-CMOD curves, denoted as $\mathcal{F}$. The process requires several hundred evaluations, however computational time can be kept relatively low by exploiting the computational efficiency provided by XFEM as well as the possibility to perform several evaluations in parallel.

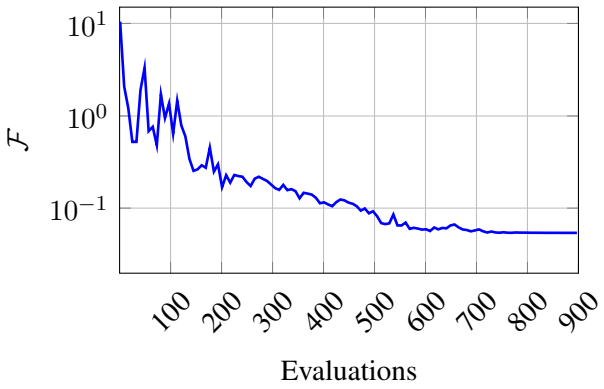

Figure 8: Performance of the CMA-ES algorithm.

5 CONCLUSIONS

A framework to identify fracture parameters of concrete was presented based on the use of XFEM as a forward simulator (computation model) and an evolutionary algorithm for solution of the inverse problem, namely the CMA-ES algorithm. An accurate representation of experimental F-CMOD curves was achieved, effectuated via the parameters identified by the proposed framework. Moreover, the identified parameters were compared against two further reference techniques, namely an inverse analysis scheme based on the analytical cracked hinge model and the fib Model Code 2010. Similar values were observed for each selected approach, yet again validating the identified parameters. The potential of the proposed numerical approach against reference techniques is emphasized to be its test-independent nature, i.e., the ability to obtain fracture parameters through any experimental results that would normally either not be eligible or would require substantial modification in current classical techniques.

The main direction of future work would be towards extending the current work to problems where analytical models are not available, and thus the proposed framework could prove advantageous. Some possibilities for such extensions would include complex geometries, mixed mode crack propagation and more complicated crack paths.

References

[1] MGGV Elices, GV Guinea, J Gomez, and J Planas. The cohesive zone model: advantages, limitations and challenges. *Engineering fracture mechanics*, 69(2):137–163, 2002.

[2] Seong Hyeok Song, Glaucio H Paulino, and William G Buttlar. A bilinear cohesive zone model tailored for fracture of asphalt concrete considering viscoelastic bulk material. *Engineering Fracture Mechanics*, 73(18):2829–2848, 2006.

[3] Julien Michels, Edmunds Zile, Christoph Czaderski, and Masoud Motavalli. Debonding failure mechanisms in prestressed cfrp/epoxy/concrete connections. *Engineering Fracture Mechanics*, 132: 16–37, 2014.

[4] Arne Hillerborg, Mats Modéer, and P-E Petersson. Analysis of crack formation and crack growth in concrete by means of fracture mechanics and finite elements. *Cement and concrete research*, 6(6):773–781, 1976.

[5] Lennart Østergaard. Early-age fracture mechanics and cracking of concrete. *Experiments and modelling. Department of Civil Engineering, Technical University of Denmark, Lyngby*, 299, 2003.

[6] Pruettha Nanakorn and Hideyuki Horii. Back analysis of tension-softening relationship of concrete. *Doboku Gakkai Ronbunshu*, 1996(544):265–275, 1996.

[7] Jan Vorel and Petr Kabele. Inverse analysis of traction-separation relationship based on sequentially linear approach. *Computers & Structures*, 212: 125–136, 2019.

[8] Victor C Li. A novel testing technique for post-peak tensile behavior of cementitious materials. *Fracture toughness and fracture energy*, pages 183–195, 1989.

[9] Volker Slowik, Beate Villmann, Nick Bretschneider, and Thomas Villmann. Computational aspects of inverse analyses for determining softening curves of concrete. *Computer Methods in Applied Mechanics and Engineering*, 195(52):7223–7236, 2006.

[10] FH Wittmann, PE Roelfstra, H Mihashi, Yiun-Yuang Huang, Xin-Hua Zhang, and N Nomura. Influence of age of loading, water-cement ratio and rate of loading on fracture energy of concrete. *Materials and structures*, 20(2):103–110, 1987.

[11] Arne Hillerborg. Stability problems in fracture mechanics testing in fracture of concrete and rock. In *International Conference on Recent Developments in the Fracture of Concrete and Rock*, pages 369–378. Elsevier, 1989.

[12] BL Karihaloo and P Nallathambi. Notched beam test: mode i fracture toughness. *Fracture mechanics test methods for concrete*, pages 1–86, 1991.

[13] E Brühwiler and FH Wittmann. The wedge splitting test, a new method of performing stable fracture mechanics tests. *Engineering fracture mechanics*, 35(1-3): 117–125, 1990.

[14] T Belytschko and T Black. Elastic crack growth in finite elements with minimal remeshing. *International Journal for Numerical Methods in Engineering*, 620(July 1998):601–620, 1999.

[15] N Moës, J Dolbow, and T Belytschko. A finite element method for crack growth without remeshing. *International Journal for Numerical Methods in Engineering*, 46 (1):131–150, 1999. ISSN 1097-0207.

[16] N Hansen, SD Muller, and P Koumoutsakos. Reducing the time complexity of the derandomized evolution strategy

with covariance matrix adaptation (CMA-ES). *Evolutionary Computation*, 11(1):1–18, 2003.

[17] A Auger and N Hansen. A restart cma evolution strategy with increasing population size. In *2005 IEEE Congress on Evolutionary Computation*, volume 2, pages 1769–1776 Vol. 2, Sept 2005. doi: 10.1109/CEC.2005.1554902.

[18] Yunus Emre Harmanci. *Long-Term Resistance of Gradient Anchorage for Prestressed CFRP Strips in Structural Concrete Retrofitting*. PhD thesis, ETH Zurich, 2018.

[19] Yunus Emre Harmanci, Julien Michels, Christoph Czaderski, Roman Loser, and Eleni Chatzi. Long-term residual anchorage resistance of gradient anchorages for prestressed cfrp strips. *Composites Part B: Engineering*, 139:171–184, 2018.

[20] Comite Europeen de Normalisation et al. Concrete-part 1: Specification, performance, production and conformity. *EN206-1, 22 CEN*, 69:23, 2000.

[21] Standard EN197 CEN. Cement-part 1: Composition, specifications and conformity criteria for common cements. *Brussels: European Commitee for Standarization*, 2008.

[22] Draft Recommendation RILEM. Determination of the fracture energy of mortar and concrete by means of three-point bend tests on notched beams. *Materials and structures*, 18(106):285–290, 1985.

[23] GV Guinea, J Planas, and M Elices. Measurement of the fracture energy using three-point bend tests: Part 1influence of experimental procedures. *Materials and Structures*, 25(4):212–218, 1992.

[24] D Rabinovich, D Givoli, and S Vigdergauz. Xfem-based crack detection scheme using a genetic algorithm. *International Journal for Numerical Methods in Engineering*, 71(9):1051–1080, 2007.

[25] H Waisman, E Chatzi, and AW Smyth. Detection and quantification of flaws in structures by the extended finite element method and genetic algorithms. *International Journal for Numerical Methods in Engineering*, 82(3):303–328, 2010. ISSN 1097-0207. doi: 10.1002/nme.2766.

[26] K Agathos, E Chatzi, and S Bordas. 3d crack detection using an xfem variant and global optimization algorithms. 2016.

[27] K Agathos, E Chatzi, and S.P.A Bordas. Multiple crack detection in 3d using a stable xfem and global optimization. *Computational Mechanics*, pages 1–18, 2018.

[28] M Duflot. A study of the representation of cracks with level sets. *International Journal for Numerical Methods in Engineering*, 70(November 2006):1261–1302, 2007.

[29] G Zi and T Belytschko. New crack-tip elements for xfem and applications to cohesive cracks. *International Journal for Numerical Methods in Engineering*, 57(15):2221–2240, 2003.

[30] N Moës and T Belytschko. Extended finite element method for cohesive crack growth. *Engineering fracture mechanics*, 69(7):813–833, 2002.

[31] A Zamani, R Gracie, and M Reza Eslami. Cohesive and non-cohesive fracture by higher-order enrichment of xfem. *International Journal for Numerical Methods in Engineering*, 90(4):452–483, 2012.

[32] L Østergaard. Early-age fracture mechanics and cracking of concrete. *Experiments and modelling. Department of Civil Engineering, Technical University of Denmark, Lyngby*, 299, 2003.

[33] FIB FIB. Model code for concrete structures 2010. 2013.

[34] J.P. Ulfkjær, S. Krenk, and R. Brincker. Analytical model for fictitious crack propagation in concrete beams. *Journal of Engineering Mechanics*, 121(1):7–15, 1995.

[35] J.F. Olesen. Fictitious crack propagation in fiber-reinforced concrete beams. *Journal of Engineering Mechanics*, 127(3): 272–280, 2001.

[36] J. Kennedy. Particle swarm optimization. In *Encyclopedia of machine learning*, pages 760–766. Springer, 2011.

[37] Arne Hillerborg. Analysis of fracture by means of the fictitious crack model, particularly for fibre reinforced concrete. 2 (4):177–184, 1980.